Growth mechanisms for TiO_2 at its rutile (110) surface

L. Vernon,[1] S. D. Kenny,[1] Roger Smith,[2,*] and E. Sanville[1]
[1]*Department of Mathematical Sciences, Loughborough University, Loughborough, LE11 3TU, United Kingdom*
[2]*FZD Rossendorf, Bautzner Landstrasse 400, D-01328 Dresden, Germany.*
(Received 20 May 2010; revised manuscript received 20 July 2010; published 9 February 2011)

Mechanisms for growth on the rutile (110) surface were investigated using a combination of *ab initio*, variable charge classical molecular dynamics and kinetic Monte Carlo (KMC) methods. *Ab initio* calculations were performed to determine relevant energy barriers, and these were used to parametrize a variable charge classical potential. Low-energy (10–40-eV) interactions of small Ti_xO_y molecules with a rutile (110) substrate were then investigated, by molecular dynamics using the variable charge potential, with the aim of determining the influence of various parameters on surface growth and defect formation. Rutile growth was simulated through sequentially depositing randomly selected atoms and molecules with energies in the tens of eV range. Long-time scale evolution was approximated through heating the substrate and through on-the-fly KMC simulations, which could be used to simulate realistic experimental deposition times. The main growth mechanism was found to involve a fast kinetic effect to subplant interstitial Ti atoms, until an O-rich surface layer formed, followed by a slower diffusion of the Ti interstitials to the O-rich surface. Bombardment at an energy of around 20 eV in an oxygen-rich atmosphere with a high proportion of bombarding TiO, TiO_2, as opposed to single atoms, was found to produce rutile growth with the best crystallinity.

DOI: 10.1103/PhysRevB.83.075412 PACS number(s): 68.55.−a, 68.35.B−, 31.15.A−, 83.10.Rs

I. INTRODUCTION

Titanium dioxide is a wide band-gap metal oxide with a large number of uses in industry. Applied as part of a multilayer coating to a glass substrate, TiO_2 is commonly used as an antireflectant[1] or self-cleaning coating,[2] but other thin-film applications include its use as a nanoparticle substrate in dye-sensitized solar cells.[3] One of the advantages of the material is that it can be produced relatively cheaply and can be deposited over large areas by using magnetron sputtering. This process can produce smooth films with a high deposition rate. Crystalline TiO_2 is most commonly found in the rutile polymorph that is the most thermodynamically stable under normal conditions but after sputter deposition films exhibiting the anatase form have also been observed.

The (110) surface of rutile, shown schematically in Fig. 1, is the most stable, and the growth kinetics have been studied experimentally with variable temperature scanning tunneling microscopy, which showed that growth on the (110) surface in an oxygen-rich environment occurs in a layer-by-layer process.[4] It was deduced that the surface grows as a result of the reaction of mobile surface-adsorbed O_2 molecules with Ti interstitials that diffuse to the surface from bulk interstitial sites. In our previous paper, a large number of surface and interstitial transition energy barriers for small molecules on and close to the rutile (110) surface were calculated[5] using both density functional theory (DFT) and a modified SMB-Q variable charge potential (Qeq) based on the formulation of Hallil *et al.*[6] The barriers found were between 1.2 and 3.5 eV for all small surface cluster transitions with the exception of transitions involving O and O_2. By contrast, O_2 diffusion could easily occur along the [001] direction in the trench between the raised O adrows on the surface. In this case, the diffusion could occur as a two-stage process with limiting barriers of 0.13 and 0.35 eV in DFT, although the variable charge potential gave a slightly higher value of 0.6 eV.

A further observation in the paper was that first-layer Ti interstitials once formed had very high energy barriers (>3 eV for both the DFT and the Qeq calculations) to transform to a Ti adatom on the pristine (110) surface but a much lower energy barrier of 1.6 eV to move in the reverse direction and that the subsurface Ti interstitial was more favorable than a Ti adatom. The results also showed that the TiO_2 unit adsorbed on the rutile (110) surface had large diffusion barriers and that, in general, there was good agreement between the barriers calculated by the modified SMB-Q potential and by DFT. However, the paper did not calculate the barriers for Ti interstitial migration to the surface in the presence of an adsorbed O_2 molecule, a process that is likely to be crucial in understanding the growth of rutile, although recent work calculated that the Ti interstitial-surface transition barriers had a limiting barrier of 1.2 eV (Ref. 7) in the presence of an O_2 admolecule. Since our preliminary calculations indicated a slightly different mechanism with a lower barrier than that reported by Wendt *et al.*[7] and the previous experimental work of Smith *et al.*[4] had reported a barrier of 0.82 eV, here, this barrier also is investigated by DFT and SMB-Q, as a precursor to performing dynamical growth simulations.

In a magnetron sputtering device, energetic particles from a plasma arrive at a surface. If the particles are charged, then the substrate bias (typically <100 eV) determines the effective arrival energy of the particles. Thus, kinetic as well as diffusional effects help determine the growth process. The growth process is also affected by the stoichiometry of the arriving particles, i.e., the mixture of particles and small molecules that arrive at the surface. To investigate the growth dynamics with DFT is beyond the scope of current computers but elevated temperature molecular dynamics (MD) and kinetic Monte Carlo (KMC) calculations of the growth of TiO_2 are possible with the SMB-Q potential. Because of the relatively good agreement between the transition barriers using the *ab initio* and classical methods, the main purpose of this

 ©2011 American Physical Society

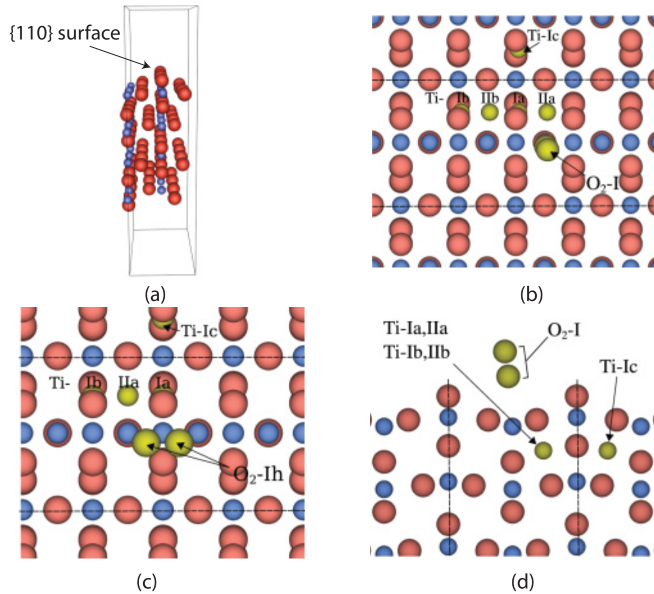

FIG. 1. (Color online) (a) The 96-atom $4 \times 2 \times 1$ cell used in the calculations and the O_2 adsorption sites together with the various stable positions for the first-layer Ti interstitials, (b), (c) viewed from above the surface showing the two different O_2 absorption sites, and (d) viewed from the [001] direction. Oxygen atoms in the crystal are red and large while Ti atoms are blue and smaller. The adsorbed atoms are yellow as indicated. In (a), the cell size is 4.9 nm × 2.2 nm × 1.2 nm, with the longer dimension perpendicular to the surface, and this includes a vacuum region of dimension 1.3 nm above and below the atoms as indicated by the box outline.

paper is an investigation of the growth mechanisms of TiO_2 as a function of the stoichiometry and energy of the arriving species using the classical potential formalism.

It is not possible to carry out growth simulations using DFT because of the limitations on computing time. Similarly, with fixed-charge potentials, it is not possible to accurately model the arrival of uncharged species onto the surface. An oxygen atom, for example, would be uncharged far from the surface but would acquire charge as it approaches the surface. However, the original SMB-Q potential was not able to model oxygen dimers correctly, predicting a repulsion between two isolated O atoms. Since in a growth process, oxygen is more likely to arrive at the surface in the form of dimers, an adaption of the potential was necessary to overcome this deficiency. This is the main principle behind our modified SMB-Q potential described in the following.

II. METHODOLOGY

A. DFT calculations

The transition barriers for the DFT calculations were performed using the climbing image nudged-elastic band (NEB) method,[8,9] with atomic forces and energies calculated using DFT under the local spin density approximation. In all calculations, a total of ten NEB images were used (including the initial and final images of each transition). The DFT calculations were performed using the PLATO suite of programs,[10,11] with pseudopotentials[12] and a triple numeric set of atom-centered basis functions with double polarization. The calculations included semicore electrons on the titanium atoms, using the same basis set and similar convergence tests as described in our previous paper.[13] The calculations were carried out using periodic boundary conditions. The supercell contained a slab of rutile with two (110) surfaces. The slab had dimensions of $4 \times 1 \times 2$ tetragonal (110) surface unit cells for all calculations (see Fig. 1) except those involving the O_2-I + Ti-iIc configuration (described later), which used a $4 \times 2 \times 2$ tetragonal cell. A Monkhorst-Pack mesh of k points was used of dimensions $1 \times 2 \times 1$ for all calculations except those involving the same O_2-I + Ti-iIc configuration, which only used the Γ point. The $4 \times 1 \times 2$ cell contains 96 atoms and, as described in our previous paper,[5] shows convergence of the binding energies to within 5%. Both the cell depth and its lateral dimension have been tested. Local-density approximation has been shown to give good results for TiO_2 and its surfaces and is used in almost all the studies of this system; see also Ref. 7.

B. Classical potential calculations

A modified form of the SMB-Q empirical potential of Hallil *et al.*[6] was implemented. This uses the variable charge equilibration (QEq) scheme[14] that iteratively minimizes the energy due to charge by performing a constrained minimization such that charges in the system sum to zero. The potential used here differs from the Hallil *et al.* form in that a short-range repulsive Ti-Ti Ziegler-Biersack-Littmark[15] interaction has been introduced, along with an attractive many-body O-O component to allow the formation and deposition of O_2 molecules since oxygen is naturally diatomic. DFT calculations have also shown that O_2 molecules on the surface are mobile and play an important role in reducing transition energy barriers for Ti interstitials.[7] The Ti hardness was modified from the original value of 12.63 to 18.3 as excessive charge transfer was originally seen when compared to equivalent processes using DFT, resulting in an artificially high Ti interstitial escape barrier.[16]

The O potential is constructed in such a way that the bulk parameters remained largely unchanged while an attractive interaction between the atoms of the molecule exists at the surface of the lattice. The way this was achieved was by the implementation of a many-body switching function (Sw) that switches between a Lennard-Jones (LJ) potential between two O atoms in the presence of no other neighbors and the Buckingham (Buck) potential of the SMB-Q potential when the O atoms are in the bulk. The parameters of the LJ potential are given by $\epsilon = 0.8$ and $\sigma = 1.05$ in the usual notation. This parameter set was a compromise as it gives a reduced binding energy of 1.6 eV for the isolated O_2 dimer (compared to 5.2 eV) but was found to be necessary to match the O_2 dissociation barrier on the surface as predicted by DFT.

The switching function itself uses the screening function (Sc) concept introduced by Baskes[17] for embedded atom calculations. Thus, the uncharged part of the O-O interaction potential is of the form

$$V_{ij} = \text{Sw} \times (\text{LJ} - \text{Buck}) + \text{Buck},$$

TABLE I. The lattice parameters, internal atom position, and bulk modulus of rutile TiO_2 calculated using the modified SMB-Q, SMB-Q empirical potentials, compared to the experiment.[19] Here, u is the O contraction parameter, and B is the bulk modulus.

Lattice parameters	Experimental[19]	Qeq	Modified QEq
a (Å)	4.59	4.63	4.80
c (Å)	2.96	2.92	2.98
u	0.305	0.302	0.300
B (GPa)	211.0	185.6	190.6

where

$$\mathrm{Sw} = \prod_{k=1}^{n} \mathrm{Sc}\,(r_{ik}) \times \prod_{k=1}^{n} \mathrm{Sc}\,(r_{jk}),$$

where r_{ik} is the interatomic separation of atoms i and k and n is the number of neighbors of i and j within the cutoff. Sc is defined by

$$\mathrm{Sc}\,(r) = \begin{cases} 1 & r < r_{\min}, \\ \frac{1}{2} + \cos\left(\frac{1}{2}\pi \frac{(r-r_{\min})}{(r_{\max}-r_{\min})}\right) & r_{\min} \leqslant r < r_{\max}, \\ 0 & r_{\max} \geqslant r, \end{cases} \quad (1)$$

where $r_{\min}$ takes the value 0.5 Å for a Ti neighbor and 1.5 Å for an O neighbor and $r_{\max}$ takes the value 2.2 Å for a Ti neighbor and 3.0 Å for an O neighbor. An in-depth discussion of the new potential including comparisons with other work is given in Ref. 18, but some basic data are given in Table I.

C. MD simulations

All MD simulations were carried out using the modified variable charge potential. Periodic boundary conditions were employed on a slab of atoms with the Coulomb interaction between the atoms calculated using Ewald summation. In order to remove the energy due to the deposited adunit, a Berendsen thermostat[20] was attached to the bottom two layers above the fixed zone. Individual and successive impacts with the surface were carried out with an initial kinetic energy of 10, 20, 30, or 40 eV being given to the adunits that were randomly oriented.

1. Single impacts

Ti, O, TiO, and TiO_2 adunits were deposited onto a lattice containing 1800 atoms. The TiO_2 slab was initially at 0 K. The adunits were started a distance of 5 Å above the surface, with the lateral position chosen randomly from an area covering one surface unit cell. For each particular energy and adunit, 1000 depositions were carried out onto the pristine (110) surface so as to accumulate sufficient statistics. The bottom two layers of the slab were fixed so as to prevent drift of the whole slab.

2. Growth simulations

Because of computing time constraints, growth was performed on a smaller 432 atom four-layer substrate at various temperatures. Each deposition was simulated until the lattice returned to the desired substrate temperature—typically about 5 ps with a 1-ps time constant in the Berendsen bath before the next arrival. Deposited atoms and molecules were randomly selected according to predefined probabilities and randomly orientated before deposition normal to the surface. The deposition energy of each species was chosen from a normal distribution with a standard deviation that was 10% of the mean energy in eV, i.e., 2 eV for a 20-eV average. Atoms that were reflected or were ejected from the surface and escaped above a certain height were removed from the simulation.

D. KMC simulations

The KMC simulation proceeds in a number of stages. At each stage of the simulation, the system is in a local minimum energy configuration, and an event list of possible transitions to a new local minimum is constructed. The best way that was found to determine the new minimum energy state was to use the relaxation and translation (RAT) method,[18] similar to the activation-relaxation technique method[21] to climb over the saddle point to the new minimum and then to tighten up on the height of the saddle (the transition energy barrier E) using the climbing image NEB method. When using a transition search algorithm, it is necessary to limit the number of atoms N in the configuration search space. This is achieved through locating deviations from the perfect lattice (referred to as a defect) and including only those atoms in the search vector that are in the neighborhood of the defect. Having constructed a vector that contains the indices of those atoms that are used by the search algorithm, the search is initialized by climbing out of the local minimum in a randomly orientated direction in $3N$-dimensional space.

A number of transition searches must be carried out before we can be confident that a representative set of energetically accessible transitions has been located; for example, Henkelman and Jønsson[22] state that when investigating Al adatom diffusion, 50 searches would be the minimum necessary to have confidence that there is an 80% probability of finding the four lowest diffusion barriers. The frequency ν of the transition is determined from the Arrhenius equation

$$\nu = \nu_0 \exp(-E/kT), \quad (2)$$

where ν_0 is a prefactor, here assumed to be 10^{13}, k is the Boltzmann constant, and T is the temperature. The sum of all the transition rates R is then determined, and a random number P is chosen between 0 and R. The chosen transition corresponds to where P falls and depends on what proportion of the interval between 0 and R is occupied by each move. Time is advanced by an increment $\delta t = -\ln u/R$ where u is another random number between 0 and 1.

While it is possible to employ a large number of searches, this can result in inefficiency since the same barriers are often found many times. It is also possible to limit the number of searches through using a time-based termination criterion. In our case, an upper limit on the search time is set, typically 20 min so that the transition searches stop when this time is exceeded or when a suitable number of unique transitions has been found. This time was chosen since it equates to about 20 separate searches using eight processors complete with relaxation and NEB calculations. At the start of the deposition, only a few unique transitions are found, but as the deposition

continues, the system becomes more complex. Thus, the time limit is a compromise between performing the simulation in a reasonable time and being sure that all relevant transitions have been found.

In order to sustain the performance of the RAT method as the configuration space increases due to the increasing numbers of deposited atoms, it was also found necessary to scale the size of the translation steps during the search algorithm. By making the maximum translational step size $\approx N^{1/2}$, consistent performance was achievable. The method was also implemented in parallel, whereby transition searches, the relaxation to the new local minimum state, and the NEB method were carried out on client machines.

The methodology described earlier will allow for modeling of the evolution of defects in a closed system. For the growth simulations, it was also necessary to introduce an external deposition event. This was achieved by adding an additional external event to the list of transitions, with the likelihood of that event being chosen dependent on the deposition frequency and the relative probabilities of the lattice transitions.

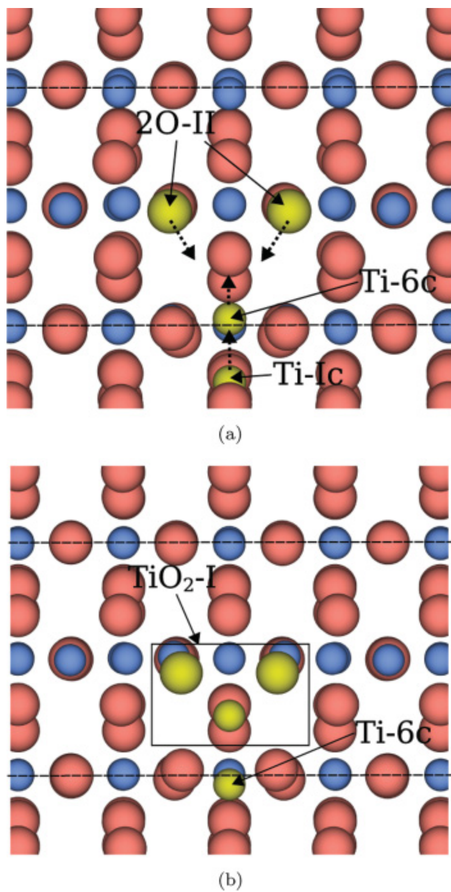

FIG. 2. (Color online) The (a) initial and (b) final configurations of the lowest-energy Ti interstitial-surface diffusion pathway looking down on the surface. The dashed lines indicate the location of the two-coordinated O adrow. The dotted arrows indicate the movement of atoms involved in the diffusion pathway. In the presence of the Ti interstitial, the O_2 unit prefers to sit flat on the surface in contrast to the isolated case shown in Fig. 1.

III. INTERSTITIAL TI DIFFUSION BARRIERS IN THE PRESENCE OF A SURFACE O_2 ADMOLECULE

In our previous paper,[5] we showed, using DFT, that although a Ti adatom on the rutile (110) surface could be bound to the raised O row, the subsurface interstitial site was energetically more favorable by 2 eV, although in order to move to this subsurface interstitial position, a barrier of 1.6 eV had to be overcome. (More recent calculations with the modified variable charge potential indicate that the direct formation of the Ti interstitial has a barrier of 0.42 eV.) In the presence of an adsorbed O_2, there are various first-layer Ti interstitial sites calculated by DFT, which are illustrated in Fig. 1. These sites are also stable positions with both the modified and the original SMB-Q potentials. The relative binding energy was calculated for each of these sites using both DFT and the new variable charge potential. By comparing these energetics to those for an adsorbed O_2 and the two types of isolated first-layer Ti interstitials, we can conclude that adsorbed O_2 binds to Ti interstitials (see Table II). Combined with the fact that the O_2 is predicted to be highly mobile along the [001] direction, even at room temperature, we can also conclude that the O_2 admolecules will tend to seek out the first-layer Ti interstitials. The DFT binding energy of the O_2-Ti interstitial system ranges between 1.29 and 1.48 eV.

In Sec. IV, the discussed results refer to the DFT calculations. The O_2 admolecule, when isolated, adopts a configuration in which the lower oxygen atom is directly above a surface five-coordinated Ti atom, while the Ti-O-O angle is approximately 120°. However, in the presence of a nearby first-layer Ti interstitial, the dioxygen can then lie down onto the surface, into a position where both of the oxygen atoms are the same height above the surface, and both are equidistant from two surface five-coordinated Ti atoms. This position, referred to as O_2-Ih here, is shown in Fig. 2 and is 0.44 eV lower in energy than when the O_2 molecule is upright. The relative energetics indicate that the O_2-Ih configuration is lower than the O_2-I configuration in the presence of a nearby first-layer Ti interstitial.

The energy difference between these two configurations ranges between 1.38 and 1.43 eV, depending upon the relative position of the first-layer Ti interstitial. The O_2-Ih admolecule can then undergo dissociation to form a set of two O adatoms

TABLE II. Energetics of Ti interstitial sites relative to the adsorbed TiO_2 unit. The energies are in eV and are relative to the adsorbed TiO_2. The site notation is defined in Figs. 1 and 2.

Configuration	DFT	Modified Qeq
Adsorbed TiO_2	0.00	0.00
O_2-I + Ti-iI a	5.88	5.92
O_2-I + Ti-iII a	5.69	5.65
O_2-Ih + Ti-iI b	4.52	5.19
O_2-Ih + Ti-iII a	4.31	4.34
O_2-Ih + Ti-iI a	4.45	5.15
O_2-Ih + Ti-iI c	5.50	4.72
2O-II + Ti-iI a	2.62	3.17
2O-II + Ti-iII a	2.74	2.43
O_2-I + isolated Ti-iI	7.17	6.12

in site II. As described in our previous paper,[5] the O-II site has the oxygen atom located nearly above a five-coordinated surface Ti atom. The dissociated state energy is lower than that of the O_2-Ih state by 0.44–1.83 eV, depending on the relative location of the first-layer Ti interstitial. Using these O_2-Ti interstitial configurations as initial and final geometries, a series of possible diffusion pathways was then examined. Each diffusion pathway examined involved three separate transitions. In each pathway, the final geometry of the transition was the TiO_2 admolecule in site TiO_2-I, [Fig. 2(b)], with no Ti interstitial defects. The energy of the final state is 5.06 eV lower than that shown in Fig. 2(a). The pathway, which has the lowest overall transition barriers, involves three steps. The first step, in which the O_2-I admolecule shifts into the O_2-Ih configuration, has a barrier of 0.06 eV. The second step, in which the O_2-Ih admolecule dissociates into 2O-II adatoms, has a barrier of 0.91 eV. The final step, shown in Fig. 2(b), in which the Ti-iI c atom replaces a six-coordinated surface Ti atom, while the six-coordinated surface Ti atom moves up into the upper hollow adsorption site, has a barrier of only 0.56 eV. This diffusion pathway is different from that reported by Wendt *et al.*,[7] where a second-layer Ti interstitial diffuses to the surface, and the barrier in our case is 0.3 eV lower. In addition, here, the adsorbed O_2 molecule dissociates before Ti diffusion onto the surface, and the replacement transition is a concerted, rather than a two-step process. The other two diffusion pathways examined, which arise from the Ti-iI a and Ti-iII a initial configurations, have much large barriers of 1.82 and 2.98 eV, respectively, and are not discussed further here. The transition also occurs with the modified variable charge potential but this time, with a slightly lower-energy barrier of 0.76 eV, whereas, with the original unmodified potential, the barrier is 1.6 eV with this transition. The two values of 0.91 and 0.76 eV straddle the reported experimental value of 0.82 eV reported by Li.[23]

The results in Table II for the modified Qeq potential show the same trend as the DFT results, whereby the binding energy of the O_2 molecule is reduced in the presence of the Ti interstitial, and the molecule prefers to be dissociated. The upright O_2 molecule is also energetically unfavorable in the presence of the interstitial.

IV. SINGLE IMPACT RESULTS

To understand the kinetics of the interaction between atoms and small molecules with the surface, a series of 1000 impacts for the different species of Ti, O, O_2, TiO, and TiO_2, at energies between 10 and 40 eV, were carried out by MD. This extends a preliminary study where a small number of impacts (50) were carried out.[13] A key feature of the single impact results is that the kinetic effects, even at the low-energy impact of 10 eV, produce no isolated Ti adatoms on the surface. Mostly first-layer Ti interstitials were formed or adunits that included both Ti and O atoms. At higher impact energies, deeper Ti interstitials can be formed. On the other hand, only a few O interstitials were formed and then, only at the higher energies of 30 and 40 eV. These generally occur as a third-layer oxygen split interstitial, but this could easily be annealed within MD time scales even at low temperatures. The deepest O interstitial observed occurred in the fourth layer as a result of a 40-eV Ti impact displacing a surface O atom. The highest number of O interstitials formed occurred for single O impacts at 40 eV with an average of 8.5% per impact occurring. At 10 eV, no O interstitials were formed for any of the impacting species. For most O and O_2 impacts, the atoms were either reflected from or adhered to the surface. However, even at an energy of 10 eV, the impacting O atom could displace a surface Ti atom at an interstitial site forming a new O adunit on the surface.

In examining the mechanism for Ti interstitial formation, it was noted that, even for single Ti atom impacts at 10 eV, over 70% of the interstitials formed from an exchange or displacement process where the incoming Ti atom took the place of a surface layer Ti which itself became interstitial. The Ti interstitials that are formed occur in the two sites previously identified by the *ab initio* calculations.[5] The average number of interstitials produced per deposition is shown in Fig. 3 for impact energies of 10 and 40 eV, and a double-atom exchange

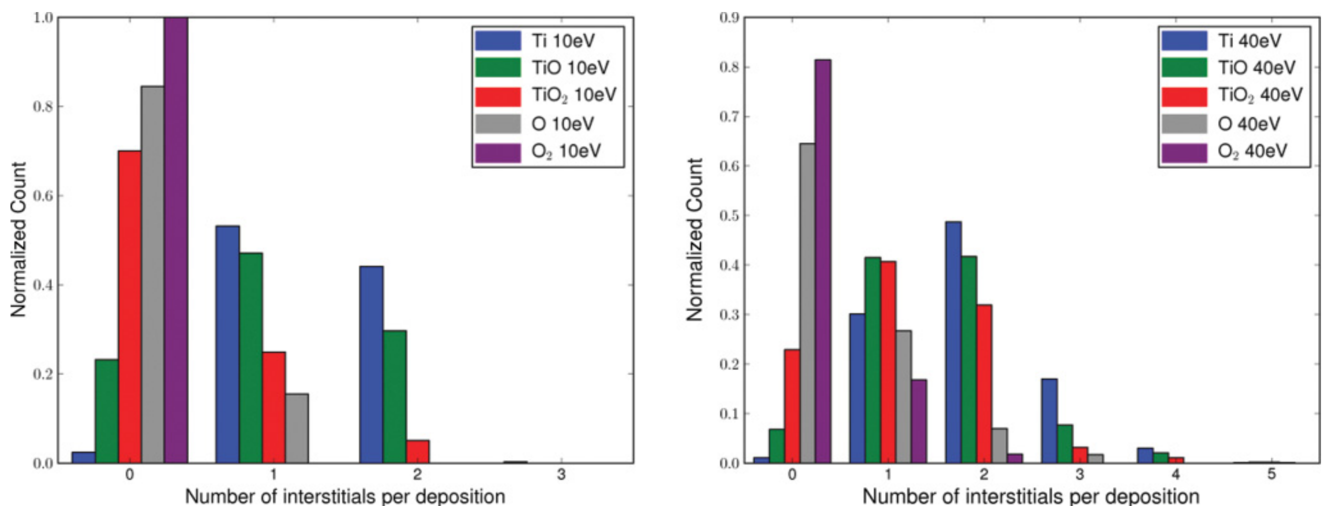

FIG. 3. (Color online) The frequency of the number of interstitials formed per impact at deposition energies of 10 eV (left image) and 40 eV (right image).

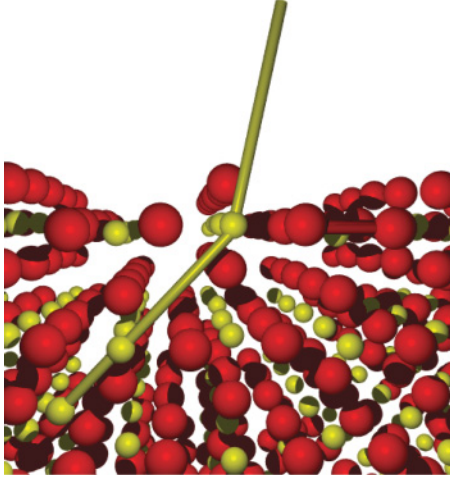

FIG. 4. (Color online) The formation of a second-layer Ti interstitial formed via a double-exchange mechanism.

mechanism for the formation of a second-layer Ti interstitial is illustrated in Fig. 4.

In order to try to classify the changes to the initially perfect crystal structure more precisely, the program NAUTY,[24] which uses graph analysis to produce a unique hexadecimal signature for each structural configuration, was used. Using NAUTY to classify structural changes automatically resulted in 3450 unique hexadecimal keys corresponding to 3450 symmetrically unique configurations. As the deposition energy increases, the classification becomes more difficult, with large numbers of defects and degrees of lattice distortion resulting in a far higher incidence of unique structures. The five different impacting species meant that 5000 distinct deposition events were performed at 10 eV, producing 5366 separate defect clusters. The total number of clusters produced exceeds the number of depositions as many depositions produced sets of defects far enough apart to be classified individually. Of those 5366 clusters, 492 were unique at 10 eV, while at 40 eV, there were a total of 6014 defect clusters of which 1740 were unique.

Despite the large number of unique configurations identified by NAUTY, the top ten unique configurations described 41.4% of the total, with the two types of Ti interstitials being the most common. These are listed in Table III.

Because of the addition of atoms to the system, vacancies occur much less frequently than interstitials. The most common vacancy that occurred was the kinetic removal of an O surface atom and the subsequent movement of a neighboring surface Ti atom into an interstitial position. Ejected or reflected O atoms occurred in only 2.3% of impacts, and Ti was never reflected or ejected. After a detailed analysis of all the various impact events by NAUTY, the most common event that occurred was the formation of a Ti interstitial; the second most common event was the formation of an O adatom, and the third most common event was the formation of a TiO_2 adunit, although this type of structure was dominated by the low-energy TiO_2 depositions. TiO adunits on the surface could also occur but were much less common than the TiO_2 adunits. The sites at which the adatoms were formed and the defects that remained

TABLE III. The top ten deviations from the perfect lattice structure due to individual impacts in order of frequency of occurrence. The interstitial classifications are the same as in Figs. 1 and 2.

Configuration	Classification
1	O adatom
2	Ti-i-I interstitial
3	TiO_2 ad-unit
4	Ti-i-II interstitial
5	Ti-i-II interstitial + O adatom
6	Reflected or sputtered O atom
7	TiO adunit
8	O surface vacancy (sputtered O) + Ti-i-II interstitial + Ti vacancy
9	Ti-i-I interstitial
10	Surface O vacancy + surface O adatom + 2 Ti vacancies + 2 × Ti-i-II interstitials

in the structure after impact were in agreement with those that were examined by the previous paper using DFT.

To summarize, therefore, the single impact analysis on the perfect rutile (110) surface has shown that, even at low energies, the kinetic effects are sufficient to overcome the formation energy barrier, and both produce large numbers of Ti interstitials while the O atoms remain bonded to the surface. TiO_2 units are also observed to form on the surface.

V. MULTIPLE SUCCESSIVE IMPACTS

Section IV, examining only single species impacts on rutile (110) has indicated that the kinetic effects during the deposition process produce a large number of subsurface Ti interstitials. For energies of around 20 eV, the kinetic effects are such that Ti interstitials are located predominantly in sites between the first layer and the second layer. As the energy is increased, the Ti penetrates more deeply, and the energy barriers for the Ti interstitials to diffuse to the surface are higher. At a 20-eV deposition energy, the O atoms and O_2 species do not penetrate the surface, and if they are not reflected, they are mobile over the surface at room temperature. The subsurface Ti interstitials can then trap the mobile O species, which in turn, causes the energy barrier for diffusion of the Ti interstitials onto the surface to be reduced, thus, allowing a new layer of crystal to grow. This is a main feature of the growth, but there are so many other complex mechanisms involved that we have yet to analyze all the various cases in detail. Instead, here, we concentrate on describing the general crystallinity of the grown layers as the deposition energy and species composition changes.

When modeling the growth of TiO_2 by MD, the realistic deposition rate will be inaccessible on the MD time scale, and as such, a standard MD simulation is not able to model multilayer growth especially well. Previous results of the simulation of growth on metal surfaces[25] using temperature-accelerated dynamics have also shown that different results can occur when simulating at experimental deposition rates compared to the faster rate using MD. In our case, a rough approximation of the correlation between computational real time and simulation time is approximately 1-fs simulated time per second of

computational time with the variable charge potential requiring more time than the fixed charge version. Given a small substrate of 432 atoms, comprising four layers that we will use in our simulations, the expected flux rate during a typical growth process is roughly ten TiO_2 units per second. To grow a single additional layer, a minimum of 36 depositions are required, corresponding to a simulation time of 3.6 s, requiring $\approx 10^6$ years of computational time. If faster deposition occurs, then it is possible that many diffusive processes could be missed. For example, we have shown that, with our modified potential, the mechanism by which a subsurface Ti interstitial recombines with a surface O_2 to form a new TiO_2 unit requires an energy barrier of 0.76 eV to be overcome. At 300 K, assuming a typical prefactor for surface processes of 10^{13} per second would mean a transition every 0.6 s and, therefore, not accessible by normal MD. If we speed up the deposition so that particles arrive more quickly, then we miss the diffusive processes. To illustrate this, some simulations were performed at room temperature at a deposition rate several orders of magnitude faster than the experiment, but also simulations were carried out at a higher temperature chosen so that the main diffusional events were accelerated in the same proportion as the enhanced deposition rate.

Deposited clusters were randomly selected according to the predefined probabilities given in Table IV and were randomly orientated before deposition normal to the surface. The proportions of the arriving species contained in this table represent different cases of mainly atomic as opposed to cluster deposition and cases where the arriving species are not stoichiometrically distributed, i.e., either oxygen rich or Ti rich. The deposition energy of each species was chosen from a normal distribution with a standard deviation that was 10% of the mean energy in eV, i.e., 2 eV for a 20-eV average. Atoms that were reflected or were ejected from the surface and escaped above a certain height were removed from the simulation.

TABLE IV. Probability of cluster selection.

Cluster	A	B	C	D	E
O	0.1	0.2	0.1	0.1	0.6
Ti	0.3	0.05	0.2	0.0	0.25
TiO	0.1	0.2	0.2	0.1	0.1
TiO_2	0.2	0.4	0.4	0.8	0.05
O_2	0.3	0.15	0.1	0.0	0.0

Sections V A–V D describe the main features of surface growth that occurs as a function of energy and temperature using MD with the accelerated deposition process.

A. 20 eV at 300 K

Growth was simulated at 300 K with a deposition energy of 20 eV, and a mix of deposition clusters was chosen with the probabilities shown in column A of Table IV. Figure 5(a) shows the growth after 200 deposition events. The crystalline form is still basically rutile, but a number of defects exists, largely in the form of Ti interstitials with some Ti vacancies. There are 21 Ti interstitials within the first six layers, of which five are within the original substrate, providing an interstitial per layer average of 3.5.

Plotting the radial density function of the grown layers against the reference substrate allows for quick quantification of the lattice disorder as can be seen in Fig. 5(a). As can be seen from the figure, the RDF indicates that the growth is not especially representative of rutile. The single impact study showed that oxygen reflection can occur at 20 eV, while Ti reflection or ejection is extremely uncommon. After 200 deposition events, the final O/Ti ratio in the deposited layer is 2.016, i.e., effectively stoichiometric taking the statistical nature of the randomized deposition event into account. Including ejected atoms in the calculation yields a O/Ti ratio

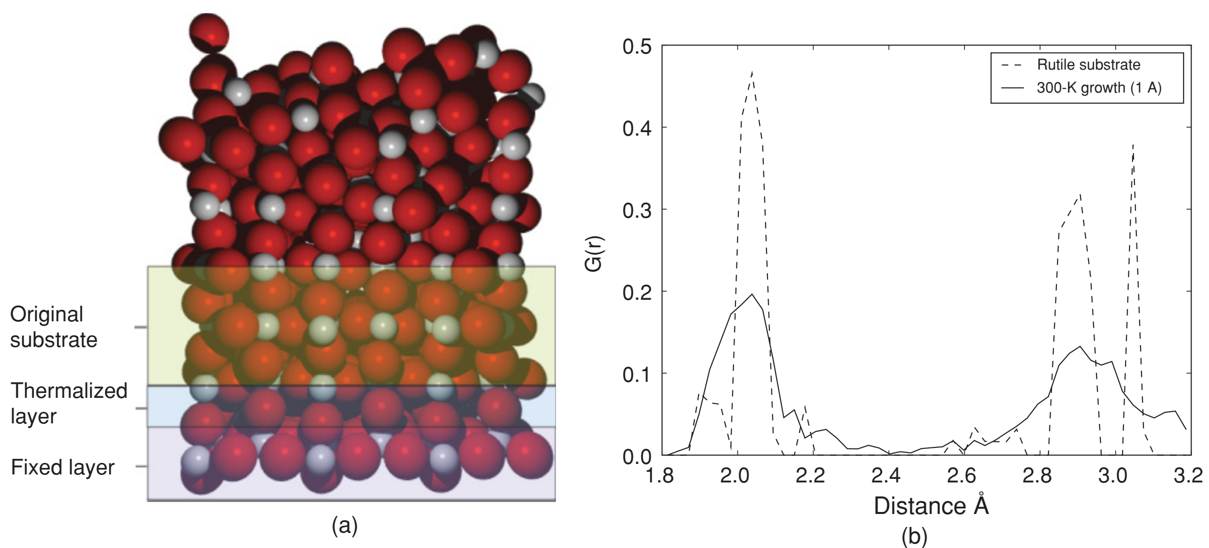

FIG. 5. (Color online) (a) The grown surface after 200 depositions at 20 eV and 300 K. In this and subsequent images, the large spheres represent O atoms, and the smaller spheres represent Ti; (b) the radial distribution function (RDF) of atoms in the grown layer, compared to the perfect rutile substrate.

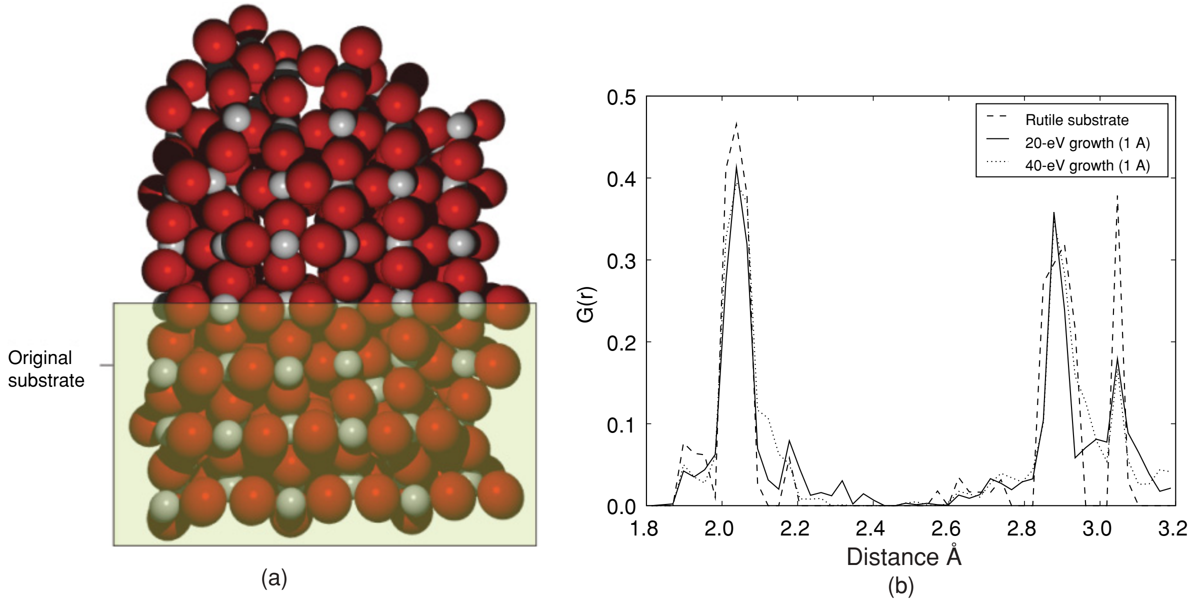

FIG. 6. (Color online) (a)The grown film after 200 deposition events at 20 eV and 1000 K; (b) the radial distribution function $G(r)$ plotted for both the rutile substrate and the atoms in the deposited film at 20 and 40 eV at 1000 K.

of 2.023, indeed, indicating a small number of oxygen atoms has been reflected. The O/Ti ratio within the top 5 Å of the lattice is high at 2.16. The surface is O rich, and there is a large number of subsurface Ti interstitials.

It is possible that the large number of interstitials and the correlated oxidization of the surface are due to the slow interstitial immobility relative to the deposition time scale. In Sec. VI, the temperature of the system is scaled such that the transition rate is accelerated proportionally with the flux rate.

B. 1000 K

A typical TiO_2 growth rate corresponds to a flux rate of 25 TiO_2 units per nm^2 per second. For the surface area of the simulated substrate, this corresponds to a flux rate of ten TiO_2 units per second. Due to computational limitations, it is necessary to use a simulated deposition time of approximately 5 ps per deposition, providing an increase in flux of 2×10^{11}. The energy barrier for Ti interstitial diffusion to the oxidized surface was found to be 0.76 eV; and, thus, 1 eV was taken as our target barrier. During a typical growth process at a temperature of 350 K, a 1-eV transition will occur with a frequency of 1.6×10^{-4} Hz, calculated from Eq. (2), assuming a fixed prefactor of 1×10^{13}. Increasing the temperature to 1000 K increases the transition rate to 9.1×10^{7} Hz. As such, the relative change in attempt frequency is 5.7×10^{11}, providing a similar scaling to the deposition flux rate.

1. Twenty electron volts

Figure 6(a) shows the rutile lattice after 200 depositions at 1000 K using the deposition conditions given in column A of Table IV. It is immediately apparent that better crystalline growth occurs for that seen at 300 K. The total number of Ti interstitials has dropped to 4, all within the original substrate, where the bottom fixed layers may be influential, yielding an interstitial per layer value of 0.57. The O/Ti ratio in the deposited layers is 2.07 from a deposited ratio of 2.08. The reduced number of interstitials correlated with the improved crystallinity of the growth supports the notion that Ti interstitial mobility to the surface plays a crucial rule in rutile growth. To verify this, the individual motion of one particular Ti atom is plotted in Fig. 7.

2. Forty electron volts

Figure 6(b) demonstrates the change in radial distribution function compared to that of the original substrate and the lattice grown at 20 eV, again using conditions A in Table IV. Although 40 eV at 1000 K yields better crystalline growth than that of 20 eV at 300 K, the interstitial-per-layer value was greater than the 20 eV at 1000 K at 0.8. Due to the increased oxygen reflection probability at 40 eV, the O/Ti ratio drops to 1.95 after only 100 deposition steps.

Since a deposition energy of 20 eV gives better crystalline growth than at 40 eV, the energy was kept constant at 20 eV for the remainder of the growth simulations.

C. Stoichiometry

In this section, the influence of the stoichiometry of incident clusters on the lattice growth was investigated. All depositions were carried out at an energy of 20 eV.

1. Low Ti

The cluster selection probability was modified to that shown in column B of Table IV providing an average O/Ti ratio of 2.31 for the depositing species. After 120 depositions, the resultant O/Ti ratio was 2.1, while the ratio within the top 5 Å was 2.5, considerably above the ratio of the depositing species. The reduced number of Ti atoms results in an oxidization of the surface, which in turn, increases the oxygen reflection during subsequent depositions. Thus, the O/Ti ratio in the substrate is self-limiting. No interstitial Ti

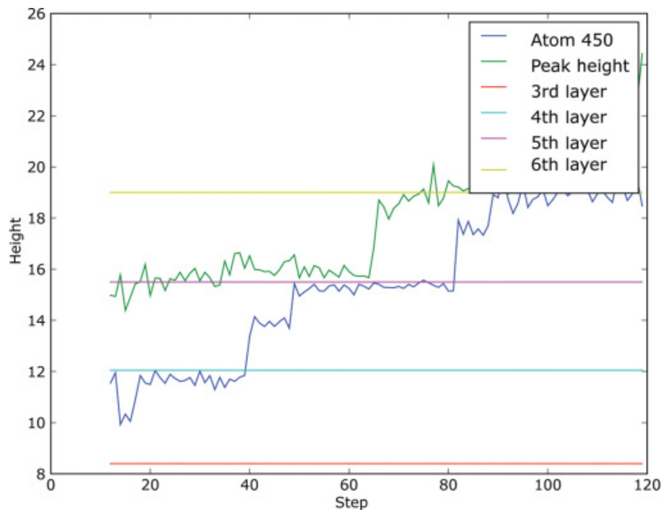

FIG. 7. (Color online) The blue (bottom) curve represents the height (in Â) of one particular chosen Ti atom as the simulation progresses. Here, the abcissa represents the number of additional units added. The green (top) curve represents the height of the top atom in the surface layer. In this case, the Ti unit always moves upward, but other examples show, as already indicated, that kinetic effects can also give motion in the other direction.

atoms remained within the lattice, and below the oxidized region, almost perfect rutile formed.

2. *Low O*

Next, the influence of O deficiency was investigated. The cluster probabilities are shown in column C of Table IV corresponding to a probabilistic O/Ti ratio of 1.625. Much poorer rutile growth occurred with 44 Ti interstitials found with the first six layers, providing an interstitial/layer ratio of 7.3 with a number of Ti vacancies also occurring. None of the deposited oxygen is reflected, hence, the resultant O/Ti ratio of 1.65 is close to the average value of the depositing species.

Due to the lack of Ti interstitials, the Ti deficient growth gives better rutile crystallinity than growth with a probabilistic O/Ti ratio of 2.0. This implies that an excess of oxygen during the growth process could result in better crystal formation.

D. Cluster deposition versus single atom deposition

In this section, we discuss the results of deposition on rutile (110) where there is a high proportion of TiO_2 species compared to the case where mainly individual atoms are deposited. Clusters were deposited with a high degree of oxygen content as shown in column D of Table IV. After 160 depositions, the O/Ti ratio was 2.02 with no oxygen reflected. After growing to eight layers, there were no residual Ti interstitials, and the rutile crystallinity was excellent.

For comparison, deposition was then carried out with more atomic than cluster species according to the ratio shown in column E of Table IV. In this case, the large proportion of incident oxygen atoms results in a corresponding increase in oxygen reflection. This is combined with initially more Ti interstitial formation. In the early growth stages, these factors produced a poor overall O/Ti ratio of 1.82 in the deposited film, while the O/Ti ratio within the top 5 Å was 2.18. Thirty-one Ti interstitials occurred within the first six layers, giving an interstitial/layer value of 5.2. The larger amount of O reflection means that more Ti interstitials form below the surface giving an interface that is similar to a Magneli phase rather than pure rutile.

VI. KMC SIMULATIONS OF GROWTH

Using the on-the-fly KMC approach, the deposition frequency could be substantially reduced, and a value of 50 Hz could be used for the same crystal size as in the MD simulations. If a deposition event was chosen, it was initialized in the same way as the MD growth modeling, with clusters randomly orientated and deposited according to a user-defined set of probabilities for species and kinetic energy. As the first few clusters were deposited, the number of potential transitions was limited, and the system was able to rapidly evolve at a rate much faster than achievable through MD. However, once the system reached sufficient complexity, the time evolution slowed due to large numbers of very low-energy barriers. Then, various transitions under 0.1 eV occur, typically involving loosely bound oxygen atoms oscillating between two or more configurations but not diffusing. At 350 K, the probability of a 0.1-eV transition occurring is 4.4×10^8 times more likely than a deposition event, thus, the KMC becomes trapped simulating the same oscillating particles moving back and forth, losing the performance benefit over classical MD.

One solution is to allow the KMC to recognize that the state has been previously visited through comparison with all previously visited configurations, thus, it is unnecessary to perform fresh transition searches, and the algorithm can reuse the old data. However, this does not provide a satisfactory performance boost as the comparison with previous configurations is a costly computational operation. As a result, the tabu blocking method was implemented.[26] The tabu transition blocking method worked well for the initial part of growth but merely acted as a stop-gap measure, extending the time scale that can be simulated before the KMC once again becomes dominated by low-energy diffusion barriers. Therefore, it was necessary to make some further approximations. The first approximation was to place a limit on the number of unique transitions per KMC step, to typically 5 or 6. Once this number had been found, no further searches were performed. This is acceptable for the early stages of the KMC simulation where there are fewer transitions but is less accurate as the system becomes more complex. Despite the limited numbers of unique transitions at each step, coupled with the tabu blocking, the system again becomes dominated by low-energy transitions that inhibit the KMC. A second approximation resolved this issue by blocking all low-energy transitions in our case all below 0.5 eV. The value of 0.5 eV was selected as a compromise that allowed for rapid evolution of the lattice while still readily containing all those barriers that were found when performing searches for simple transitions on the lattice surface. The third approximation was the form of cluster selection. Loosely tethered oxygen atoms were found to be the primary source of low-energy barriers, being able to vibrate between configurations at extremely high frequencies.

In order to restrict the number of oscillating oxygen atoms, the probability of cluster selection was altered such that only complete TiO_2 units were deposited during the MD stages of the KMC.

A. Results

Using the previous conditions, it became possible to simulate multilayer growth of TiO_2 through on-the-fly-KMC. Figure 8 shows the radial distribution function of the grown lattice after 130 KMC steps compared to an accelerated MD simulation with the same number of added particles at a temperature of 300 K. Images of the structure also show near-perfect rutile growth. While KMC simulated approximately 1.3 actual seconds, the MD simulation modeled just 1.2×10^{-10} s. With a deposition frequency of TiO_2 50 units per second, the probability of a deposition occurring became similar to a transition of 0.8 eV being selected at 350 K. It took approximately 1-week computational time running on eight processors to provide 1.3-s simulated time for the KMC results.

A snapshot of the KMC is given to provide insight into the global behavior. The growth after 30 KMC steps is shown in Fig. 9(a), and the transition to a more ordered structure is shown in Fig. 9(b). Note that the surface contains no Ti atoms and is not uniformly covered with oxygen. In this case, there is a cluster of O atoms that transforms to a more ordered structure after the transition. The KMC code found six unique transitions from the configuration shown in Fig. 9(a) with barriers of 0.60, 0.69, 0.96, 1.29, 1.78, and 1.85 eV, and, as might be expected, the lowest-energy barrier was chosen for the transition. Typically, the method uses between about 150 and 450 evaluations of the potential energy of the system per transition.

Therefore, the example shows that OTF-KMC simulations of film growth for realistic times is possible provided that the processes are not dominated by large numbers of low-energy barriers. The transition shown in Fig. 9 is one example of a large number of complex transitions that can occur as the surface becomes covered with O atoms. Although these transitions are too numerous to list, the resulting structures that eventually form show good crystallinity, indicating that, despite the complex rearrangements of atoms in the structure, the fundamental principle of Ti interstitial formation followed by upward motion to the surface is the dominant growth mechanism.

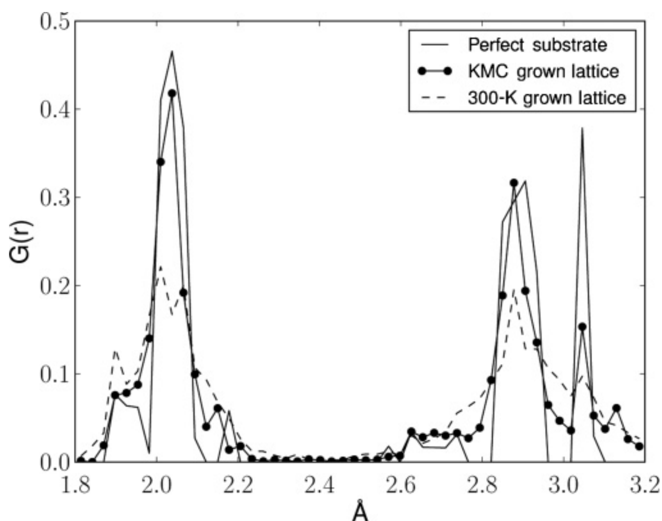

FIG. 8. The radial distribution function for the KMC simulations after 130 steps, compared to that of the perfect rutile lattice and the 300-K accelerated MD simulations.

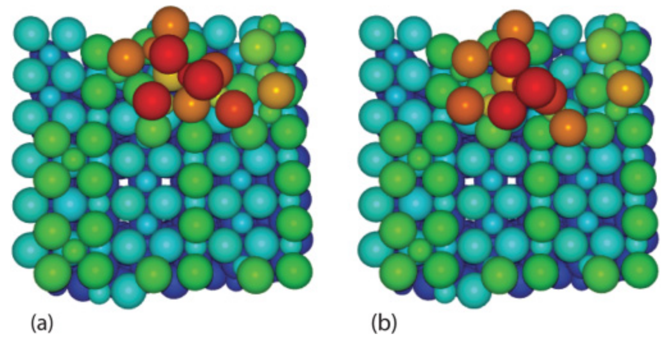

FIG. 9. (Color online) An example of a concerted motion of O adatoms with a barrier of 0.6 eV, during growth where the rutile (110) surface is viewed from above. (a) The crystal surface after 30 KMC steps and (b) after the combined motion of a number of surface O atoms. Here, the larger spheres represent O, and the smaller spheres represent Ti. Coloring of the atoms is, with distance for the viewer, blue → green → red.

VII. CONCLUSIONS

Three different approaches have been used to identify the growth mechanisms on rutile (110) as a result of low-energy impacts of atoms and small molecules with the *ab initio* results being used to parametrize the variable charge potential. Thus, the modified Hallil *et al.* potential provides a sensible dynamical behavior for the growth processes for the rutile polymorph of TiO_2. In identifying the growth process, all techniques point to the same conclusion. Kinetic effects produce subsurface interstitial Ti, while the O atoms remain on the surface. Once oxidized, the surface can attract the subsurface interstitial from the bulk to form the next crystalline layer. This is in line with previous experimental evidence that oxidized surfaces can attract Ti interstitials from the bulk.[27] None of the methods indicates that oxygen vacancies play a role in the growth process so that we have not discussed these in detail. However, calculations on isolated subsurface oxygen vacancies indicate that they have a diffusion barrier in excess of 1.6 eV.

Optimized deposition parameters for the best crystalline growth have also been found with the best crystals forming with an impact energy of around 20 eV and an excess of O. An excess of oxygen is not damaging as the stoichiometry is self-limiting with excess oxygen being reflected as the surface becomes oxidized. Growth at 20 eV is superior to that at 40 eV due to the reduced penetration depth of the Ti atoms. Ti atoms are mobile in directions both toward the surface and away from it. Often, Ti atoms form as subsurface interstitials either by being displaced from the surface layer or by direct implantation. Once the surface is

O rich, these Ti interstitials move in the opposite direction to form a new crystalline layer. Thus, the mobility of Ti interstitials is crucial to the rutile growth process. Accelerating the dynamics of the simulation through heating the substrate allowed the Ti subsurface interstitial atoms to migrate onto the surface either directly or via an exchange within the deposition time frame making growth simulation using MD possible.

By filtering out low transition energy barriers that do not result in the net diffusion of atoms in the crystal or over the surface, OTF-KMC simulations of the growth process were possible at normal deposition temperatures for realistic experimental time frames. The results of these simulations showed a similar good grown crystallite as temperature accelerated growth with a large number of different and complex processes occurring during the growth process but support the main conclusion regarding the principal growth mechanism.

ACKNOWLEDGMENTS

The authors would like to thank J. M. Walls and P. Mulheran for many useful discussions. The work was supported by the EPSRC materials modeling Grant No. EPC524322/1. Use of the UK's HPCX computer resources and Loughborough University's high-performance computing systems are also gratefully acknowledged. R. Smith would also like to acknowledge support from the Royal Academy of Engineering Foundation (UK).

---

[*]Permanent address: Department of Mathematical Sciences, Loughborough University, Loughborough, LE11 3TU, U.K.

[1]B. S. Richards, S. F. Rowlands, C. B. Honsberg, and J. E. Cotter, Prog. Photovoltaics **11**, 27 (2002).
[2]C. J. W. Ng, H. Gao, and T. T. Y. Tan, Nanotechnology **19**, 445604 (2008).
[3]M. K. Nazeeruddin, T. Bessho, L. Cevey, S. Ito, C. Klein, F. D. Angelis, S. Fantacci, P. Comte, P. Liska, and H. Imai, J. Photochem. Photobiol., A **185**, 331 (2007).
[4]R. D. Smith, R. A. Bennett, and M. Bowker, Phys. Rev. B **66**, 035409 (2002).
[5]E. J. Sanville, L. J. Vernon, S. D. Kenny, R. Smith, Y. Moghaddam, C. Browne, and P. Mulheran, Phys. Rev. B **80**, 235308 (2009).
[6]A. Hallil, R. Tetot, F. Berthier, I. Braems, and J. Creuze, Phys. Rev. B **73**, 165406 (2006).
[7]S. Wendt, P. Sprunger, E. Lira, G. Madsen, J. H. Z. Li, J. Matthiesen, A. Blekinge-Rasmussen, E. Laegsgaard, B. Hammer, and F. Besenbacher, Science **320**, 1755 (2008).
[8]G. Henkelman and H. Jønsson, J. Chem. Phys. **113**, 9978 (2000).
[9]G. Henkelman, B. P. Uberuaga, and H. Jønsson, J. Chem. Phys. **113**, 9901 (2000).
[10]S. D. Kenny, A. P. Horsfield, and H. Fujitani, Phys. Rev. B **62**, 4899 (2000).
[11]S. D. Kenny and A. P. Horsfield, Comput. Phys. Commun. **180**, 2616 (2009).
[12]C. Hartwigsen, S. Goedecker, and J. Hutter, Phys. Rev. B **58**, 3641 (1998).
[13]L. J. Vernon, R. Smith, and S. D. Kenny, Nucl. Instrum. Methods Phys. Res. B **267**, 3022 (2009).
[14]A. Rappe and W. Goddard III, J. Phys. Chem. **95**, 3358 (1991).
[15]J. F. Ziegler, J. P. Biersack, and U. Littmark, *The Stopping and Range of Ions in Matter* (Pergamon, New York, 1985).
[16]P. Mulheran, C. Browne, and Y. Moghaddam, Mol. Simul. **35**, 532 (2008).
[17]M. I. Baskes, Mater. Chem. Phys. **50**, 152 (1997).
[18]L. J. Vernon Ph.D. thesis, Loughborough University, 2010.
[19]S. C. Abrahams, J. Chem. Phys. **55**, 3206 (1971).
[20]H. Berendsen, J. Postma, and W. Van Gunderstan, J. Chem. Phys. **81**, 3684 (1984).
[21]G. Barkema and N. Mousseau, Comput. Mater. Sci. **20**, 285 (2001).
[22]G. Henkelman and H. Jønsson, in *Atomistic Aspects of Epitaxial Growth*, edited by M. Kotrla (Kluwer, Dordrecht, 2002), p. 63.
[23]M. Li, Surf. Sci. **437**, 173 (1999).
[24]B. McKay, Congr. Numer. **30**, 45 (1981).
[25]J. A. Sprague, F. Montalenti, B. P. Uberuaga, J. D. Kress, and A. F. Voter, Phys. Rev. B **66**, 205415 (2002).
[26]F. Glover and M. Laguna, *Tabu Search* (Kluwer, Dordrecht, 1997).
[27]P. Stone, R. A. Bennett, and M. Bowker, **1**, 1.1 (1999).